Applied Thermal Engineering 29 (2009) 3542–3551

Contents lists available at ScienceDirect

Applied Thermal Engineering

journal homepage: www.elsevier.com/locate/apthermeng

Development and validation of a condenser three zones model

Cristian Cuevas [a,*], Jean Lebrun [b,1], Vincent Lemort [b,2], Philippe Ngendakumana [b,3]

[a] Departamento de Ingeniería Mecánica, Facultad de Ingeniería, Universidad de Concepción, Casilla 160-C, Concepción, Chile
[b] Thermodynamics Laboratory, University of Liège, Campus du Sart Tilman – Bâtiment B49, Parking P33, B-4000 Liège, Belgium

ARTICLE INFO

Article history:
Received 10 February 2009
Accepted 7 June 2009
Available online 10 June 2009

Keywords:
Air-cooled condenser
Modelling
Critical pressure
R134a

ABSTRACT

A general and simple "deterministic" model of a refrigeration condenser is presented. The model assumes that the condenser can be divided into three distinct zones on the refrigerant side: the vapour de-superheating zone, the two-phase zone and the sub-cooled liquid zone.

The model inputs are the air supply temperature, the air mass flow rate, the refrigerant supply temperature (or the over-heating), the exhaust sub-cooling and the refrigerant mass flow rate. The model is able to identify the pressures and temperatures in each zone and the corresponding heat flows. The model also gives the geometrical repartition among the zones and the pressure drop on air-side.

The condenser model is validated with a total of 183 tests. Testing conditions cover a very wide domain, including pressures up to 40 bars with refrigerant R134a. The model is able to predict with a probability of 95% the condenser supply pressure within a confidence interval of +0.5 and −0.1 bar. This means a condenser power confidence interval within −200 and +100 W, which is considered here as acceptable. Refrigerant pressure drop is predicted with a higher error, but it is attributed to measuring uncertainty. On the other hand, air pressure drop is predicted with a very poor accuracy. Undoubtedly, this is due to the friction factor correlation used in this study which is not the most adequate. Here a difference of 40% is obtained.

1. Introduction

This study considers a classical refrigeration system, which works at high temperature and pressure levels in both the evaporator and the condenser. In the application considered, the main technical challenges are the high temperature levels at the exhaust of the compressor, and the reduced cross-section space available for the condenser. The results presented here are focused on the condenser modelling.

The main fact to be considered in the modelling is the co-existence of three refrigerant phases: refrigerant enters in a gaseous state, goes through a two-phase state and finally leaves the condenser in a liquid state.

The simplest model considers these three zones as one lumped two-phase zone, where only one global heat transfer coefficient is calculated or identified [2].

A more detailed model distinguishes between the different zones and identifies a specific heat transfer coefficient for each zone. This second approach is better, because it allows verifying the separate influences of gaseous, two-phase and liquid zones on the heat exchanger performance.

With respect to the modelling, there exists two ways to simulate the heat exchangers: either using a "deterministic" model or using a "theoretical–experimental" model.

The "deterministic" model is generally used when the heat exchanger geometry is known or in the case of heat exchanger sizing. This model can also be used to identify heat transfer or frictions factor correlations.

Fischer and Rice [11] developed a quite complete "deterministic" model that considers the three zones and the condenser geometry. The use of this model requires a detailed knowledge of the condenser geometry. This kind of model allows predicting the condenser performance almost without any experiment or catalogue data.

On the other hand, the "theoretical–experimental" model is used when the heat exchanger geometry is not known and when the heat exchanger performance is known at the nominal conditions or at several conditions. Usually this approach uses some parameters to fit the manufacturer or experimental results with the simulated ones, as in Cuevas et al. [8].

Kempiak and Crawford [16] developed a "theoretical–experimental" three-zoned model, considering the condenser geometry only for the pressure drop model. In their model, the heat transfer coefficients are determined as function of the refrigerant and

* Corresponding author. Tel.: +56 41 2203550; fax: +56 41 2251142.
E-mail addresses: crcuevas@udec.cl (C. Cuevas), j.lebrun@ulg.ac.be (J. Lebrun), vincent.lemort@ulg.ac.be (V. Lemort), pngendakumana@ulg.ac.be (P. Ngendakumana).
[1] Tel.: +32 4 3664801; fax: +32 4 3664812.
[2] Tel.: +32 4 3664824; fax: +32 4 3664812.
[3] Tel.: +32 4 3664803; fax: +32 4 3664812.

1359-4311/$ - see front matter © 2009 Elsevier Ltd. All rights reserved.
doi:10.1016/j.applthermaleng.2009.06.007

Nomenclature

A	area (m^2)
AU	heat transfer coefficient ($W\,K^{-1}$)
c	specific heat ($J\,kg^{-1}\,K^{-1}$)
F	fin (–)
f	friction factor (–)
h	enthalpy ($J\,kg^{-1}$) or heat transfer coefficient or ($W\,m^{-2}\,K^{-1}$) or height (m)
$\dot{H}$	enthalpy flow (W)
K	factor (–)
k	conductivity ($W\,m^{-1}\,K^{-1}$)
l	length (m)
L	louver (–)
$\dot{M}$	mass flow rate ($kg\,s^{-1}$)
m	fin effectiveness parameter (–)
P	pressure (Pa or bar) or perimeter (m)
$\dot{Q}$	heat flow (W)
R	thermal resistance ($K\,W^{-1}$)
Re	Reynolds number (–)
t	temperature (°C) or thickness (m)
T	absolute temperature (K) or tube (–)
x	vapour quality (–)

Greek symbols

α	area ratio (–)
ε	effectiveness or uncertainty (–)
θ	angle (°)
σ	standard deviation or ratio of free-flow area to frontal area (–)

Subscripts

a	air
b	base
c	contraction or cross-sectional
cd	condenser
cf	cold fluid
d	depth
e	expansion
ex	exhaust
f	frontal or friction or fin or finned
g	gas or global
lub	lubricant
$meas$	measured
min	minimal
oh	overheating
p	pitch
r	refrigerant
sc	subcooling or subcooled
sh	superheated
su	supply
tp	two-phase

airflow rate. The model can be applied to any condenser; it is necessary to know only the refrigerant side geometry.

More simplified two-zoned models can also be found in the literature, like the model proposed by Reichler [18]. This model needs an experimental or catalogue database to determine three parameters which are used to calculate the heat transfer coefficient.

In the present study, the condenser is modelled in three zones, by using the "deterministic" approach. The geometry of the condenser is well known and heat transfer coefficients are calculated by using correlations from the literature.

2. Condenser modelling

A simplified approach for the condenser modelling is proposed hereafter. Whatever the condenser may be, the modelling is simplified by using one of the following three configurations: pure *counterflow*, pure *crossflow* or combination of both, as shown in Figs. 1–3, respectively. In this modelling the condenser is divided into three zones: vapour de-superheating, two-phase and subcooled zone. It is assumed that the fluids are homogenously distributed among tubes on the refrigerant side and on the frontal surface on the air-side. The lubricant is not supposed to affect heat transfer coefficient, but it is taken into account in the energy balance.

Heat transfer and pressure drops are calculated as indicated hereafter.

2.1. Heat transfer

2.1.1. Vapour de-superheating zone

The steady-state thermal balance of the de-superheating zone is given by the following equation:

$$\dot{H}_{r,cd,sh} + \dot{H}_{\mathrm{lub},cd,sh} - \dot{H}_{cf,cd,sh} = 0 \tag{1}$$

where the enthalpy flow rates are given by:

Refrigerant enthalpy flow rate

$$\dot{H}_{r,cd,sh} = \dot{M}_{r,cd,sh} \cdot (h_{r,su,cd,sh} - h_{r,ex,cd,sh}) \tag{2}$$

Lubricant enthalpy flow rate

$$\dot{H}_{\mathrm{lub},cd,sh} = \dot{M}_{\mathrm{lub},cd,sh} \cdot c_{\mathrm{lub},cd,sh} \cdot (t_{\mathrm{lub},su,cd,sh} - t_{\mathrm{lub},ex,cd,sh}) \tag{3}$$

Cold fluid enthalpy flow rate

$$\dot{H}_{cf,cd,sh} = \dot{M}_{cf,cd,sh} \cdot (h_{cf,ex,cd,sh} - h_{cf,su,cd,sh}) \tag{4}$$

Lubricant flow rate is supposed to be imposed by the compressor [9] and it is considered as an input in the present model. Moreover, it is assumed to be in equilibrium at the condenser supply and exhaust, and that there is no lubricant accumulation in the compressor, in the heat exchangers and in the lines.

The fluid to fluid heat transfer is calculated by using the ε-NTU method:

$$\dot{H}_{r,cd,sh} = \varepsilon_{cd,sh} \cdot \dot{C}_{\min,cd,sh} \cdot (t_{r,su,cd,sh} - t_{cf,su,cd,sh}) \tag{5}$$

It must be remarked, in Eqs. (2)–(5), that $\dot{M}_{r,cd,sh} = \dot{M}_{r,cd}$ for the three possible arrangements defined in Figs. 1–3.

For *counterflow* and combined *counterflow*/*crossflow* arrangements, the cold fluid mass flow rate is equal to the inlet mass flow rate, $\dot{M}_{cf,cd,sh} = \dot{M}_{cf,cd}$.

On the other hand, for the *crossflow* arrangement, the cold fluid mass flow rate can be defined as follows [7]:

$$\dot{M}_{cf,cd,sh} = \alpha_{cd,sh} \cdot \dot{M}_{cf,cd} \tag{6}$$

where $\alpha_{cd,sh}$ is the fraction of the total cold fluid mass flow rate which circulates through the de-superheating zone. Assuming a homogeneous frontal cold fluid distribution, the fraction $\alpha_{cd,sh}$ is given by the following equation:

$$\alpha_{cd,sh} = \frac{A_{f,cd,sh}}{A_{f,cd}} \tag{7}$$

where $A_{f,cd,sh}$ is the frontal area utilized for the de-superheating zone and $A_{f,cd}$ is the total frontal area.

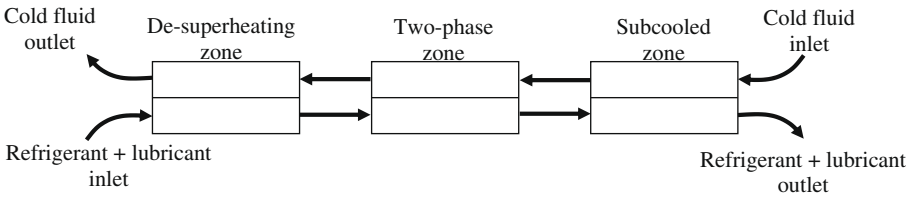

Fig. 1. *Counterflow* arrangement.

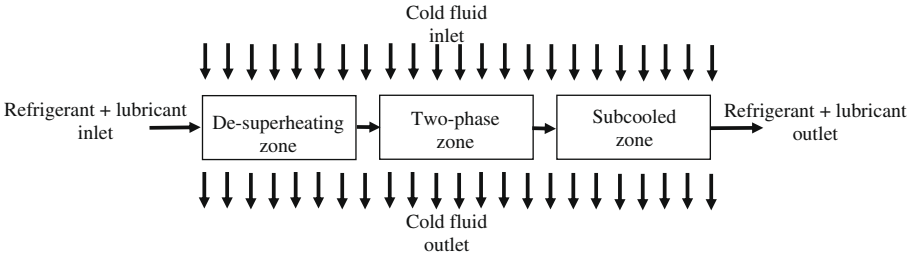

Fig. 2. *Crossflow* arrangement.

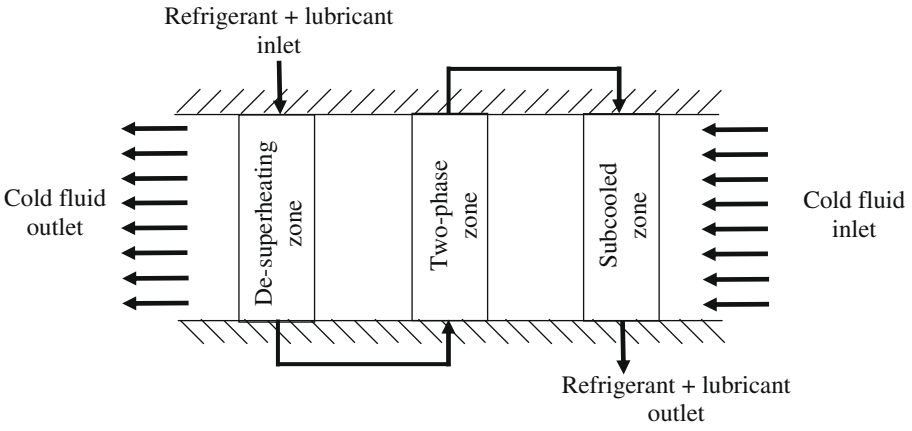

Fig. 3. Combined *counterflow* and *crossflow* arrangement.

If the heat exchanger geometry is uniform all along the cold-fluid side, the frontal areas can be related to the heat transfer areas by the following relationship:

$$\alpha_{cd,sh} = \frac{A_{cf,cd,sh}}{A_{cf,cd}} = \frac{A_{r,cd,sh}}{A_{r,cd}} \tag{8}$$

where $A_{cf,cd,sh}$ is the cold side heat transfer area of the de-superheating zone, $A_{cf,cd}$ the total cold side heat transfer area, $A_{r,cd,sh}$ the refrigerant side heat transfer area of the de-superheating zone, and $A_{r,cd}$ is the total refrigerant side heat transfer area.

The de-superheating heat exchanger effectiveness is computed, either by the counterflow or the crossflow relationships given in the literature, as function of the *NTU* and of the flow capacity ratio.

Here, the global heat transfer coefficient *AU* is defined by the following relationship:

$$\frac{1}{AU_{cd,sh}} = \frac{1}{A_{r,cd,sh} \cdot h_{r,cd,sh}} + R_{m,cd,sh} + \frac{1}{\eta_{g,cf,cd,sh} \cdot A_{cf,cd,sh} \cdot h_{cf,cd,sh}} \tag{9}$$

The overall surface effectiveness ε is calculated knowing the finned heat transfer area, the base-heat transfer area and the fin effectiveness, according to the following equation:

$$\varepsilon = 1 - \left[\frac{A_f}{A_b + A_f}(1 - \varepsilon_f)\right] \tag{10}$$

For the fin effectiveness, the relationship for a thin, straight fin of uniform rectangular section with constant one-dimensional conduction is considered. The adiabatic tip fin hypothesis is used: fins are sandwiched between two flat tubes that are considered to be at the same temperature (see Fig. 8). The relationships utilized to calculate it are the followings [14]:

$$\varepsilon_f = \frac{tanh(m \cdot L_f)}{m \cdot L_f} \tag{11}$$

$$m = \sqrt{\frac{h \cdot P_f}{k_f \cdot A_{c,f}}} \tag{12}$$

In this condenser the refrigerant circuitry is divided in five paths. Considering Fig. 4, there are several possibilities for the de-superheating length.

In all cases, it is proposed to calculate the de-superheating heat transfer coefficient as follows:

$$AU_{cd,sh} = AU_{cd,sh,1} + AU_{cd,sh,2} + AU_{cd,sh,3} + \cdots\cdots\cdots + AU_{cd,sh,n} \tag{13}$$

For each path, the refrigerant properties are calculated at the average temperature and pressure between inlet and outlet of the de-superheating zone.

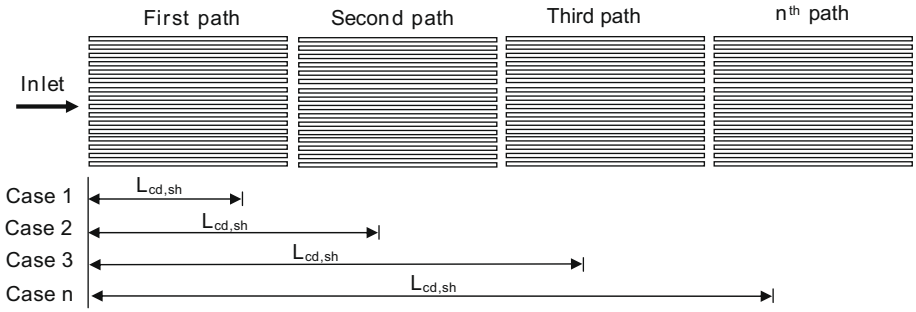

Fig. 4. Refrigerant circuitry.

2.1.2. Two-phase zone

Heat transfer in this zone is given by the same three equations as for the vapour de-superheating zone. The main difference is the effectiveness, which is calculated as for a semi-isothermal heat exchanger.

For the two-phase zone, an average heat transfer coefficient is used, which is here calculated by using the following equation:

$$\bar{h}_{tp} = \frac{1}{x_2 - x_1} \int_{x_1}^{x_2} h_{tp}(x)dx \tag{14}$$

In the case of the condenser $x_1 = 1$ and $x_2 = 0$.

The global heat transfer coefficient is also defined in the same way as for the de-superheating zone.

2.1.3. Subcooled liquid zone

The same method as for the vapour de-superheating zone is considered for this zone, with the effectiveness again computed using the relationships proposed for a crossflow or a counterflow configuration.

The heat transfer coefficients are calculated at the average conditions.

2.1.4. Globalization

The condenser power is finally calculated with the following equations:

$$\dot{H}_{cf,cd} = \dot{H}_{cf,cd,sh} + \dot{H}_{cf,cd,tp} + \dot{H}_{cf,cd,sc} \tag{15}$$

$$\dot{H}_{r,cd} = \dot{H}_{r,cd,sh} + \dot{H}_{r,cd,tp} + \dot{H}_{r,cd,sc} \tag{16}$$

$$\dot{H}_{cf,cd} = \dot{H}_{r,cd} + \dot{H}_{\mathrm{lub},cd} \tag{17}$$

2.2. Pressure drop

Here, the pressure drop is calculated as follows:

$$\Delta P = \Delta P_{in,port} + \Delta P_{in,core} + \Delta P_{m,core} + \Delta P_{f,core} + \Delta P_{out,core} + \Delta P_{out,port} \tag{18}$$

where $\Delta P_{i,port}$ is the inlet or outlet port pressure drop (i = inlet or outlet), $\Delta P_{in,core}$ is the core inlet pressure drop, $\Delta P_{m,core}$ is the core pressure variation due to fluid density change, $\Delta P_{f,core}$ is core friction pressure drop and $\Delta P_{out,core}$ is the core outlet pressure rise.

This formulation is applicable on both refrigerant and cold-fluid sides.

2.3. Information flow diagram

Fig. 5 shows the inputs, outputs and parameters of the condenser model.

As explained previously, in the "deterministic" model the parameters are the heat exchanger geometry and the correlation issues from the literature to calculate the heat transfer coefficients and the pressure drops. The main outputs of the model are the condenser supply pressure, the refrigerant side pressure drop and the air-side pressure drop. The others outputs shown in Fig. 5 are derived from these main outputs.

3. Experimental set-up

3.1. Condenser description

In the present study, a louvered fin-and-tube condenser composed of an arrangement of five heat exchangers, connected in

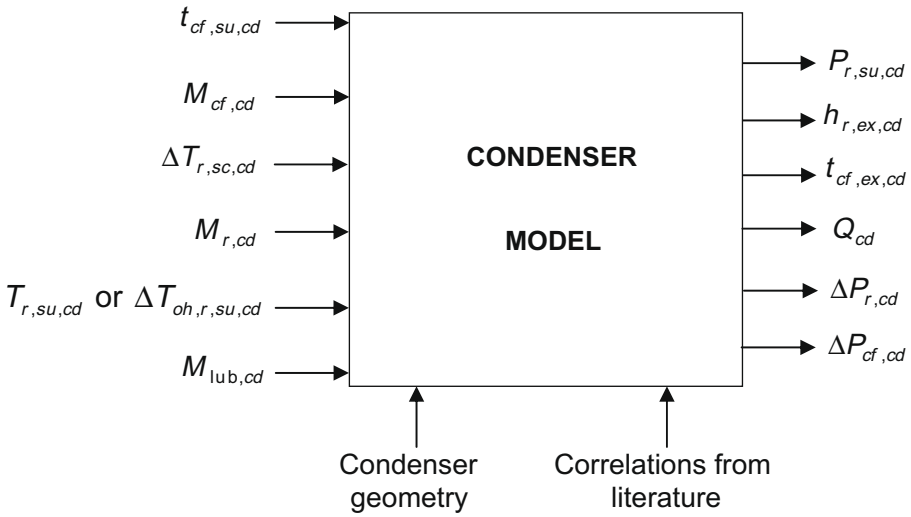

Fig. 5. Definitions of the condenser inputs, outputs and parameters.

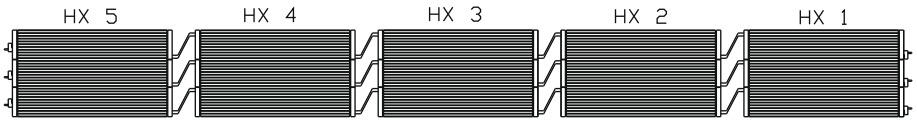

Fig. 6. Condenser used in the validation of the model.

Table 1
Heat exchanger characteristics.

Internal cross-sectional area (mm^2)	11.12
Internal heat transfer area (m^2)	0.644
Internal hydraulic diameter (mm)	1.322
Frontal area (m^2)	0.249
Frontal free-flow area (m^2)	0.188
Ratio free-flow to frontal area	0.76
Finned area (m^2)	4.709
External unfinned area (m^2)	0.622
External total area (m^2)	5.331

Table 2
Fin characteristics.

T_p: 12 mm
T_d: 16 mm
T_h: 2 mm
F_p: 1.3 mm
F_d: 15.5 mm
F_h: 10 mm
F_t: 0.16 mm
L_h: 0.8 mm
L_l: 8 mm
L_p: 1.5 mm
θ: 30°

series on the refrigerant side (see Fig. 6), is characterized experimentally. The main geometrical characteristics of this condenser are given in Table 1 and for the fin characteristics in Table 2. Fig. 7 gives complementary information for the fin nomenclature.

On the refrigerant side, the condenser uses flat extruded aluminium tubes with membranes with the dimensions given in Fig. 7.

This condenser uses a combination of a local *crossflow* and global *counterflow* arrangement. Thus, the adequate modelling is that shown in Fig. 3.

3.2. Test bench description

The condenser is installed in a closed air loop which is composed of a centrifugal fan, a damper, a series of three cooling coils and a set of four nozzles, mounted in parallel for the air-flow measurement (Fig. 9). The cooling coils and the damper allow setting, respectively, the air temperature and the air-flow rate at condenser supply. As the dimensions of the duct are bigger than the condenser dimensions, the condenser inlet section is reduced using a convergent section to have an uniform air velocity profile.

The following measurements are developed:

(a) on the air-side: air-flow rate, supply and exhaust temperatures and pressure drop;

(b) on the refrigerant side: supply and exhaust pressures and temperatures.

The refrigerant mass flow rate is determined from the evaporator steady-state thermal balance, with an uncertainty estimated,

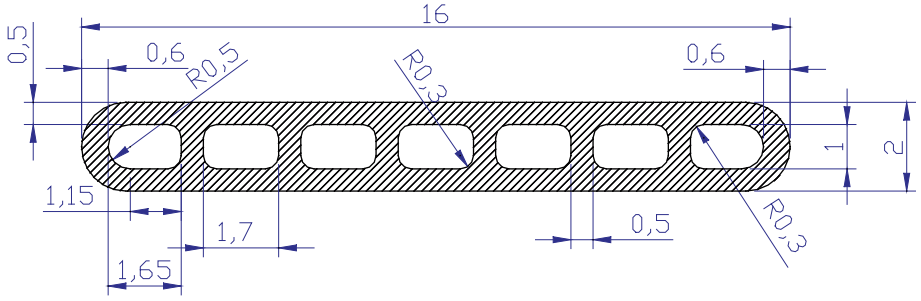

Fig. 7. Tube geometry (dimensions in mm).

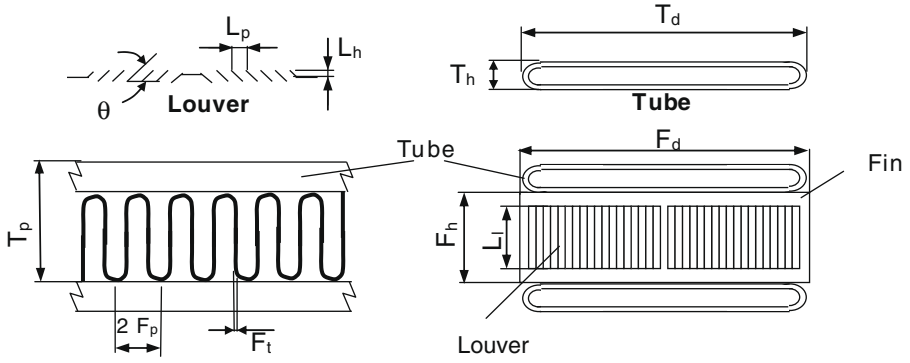

Fig. 8. Louvered fin-and-tube geometry.

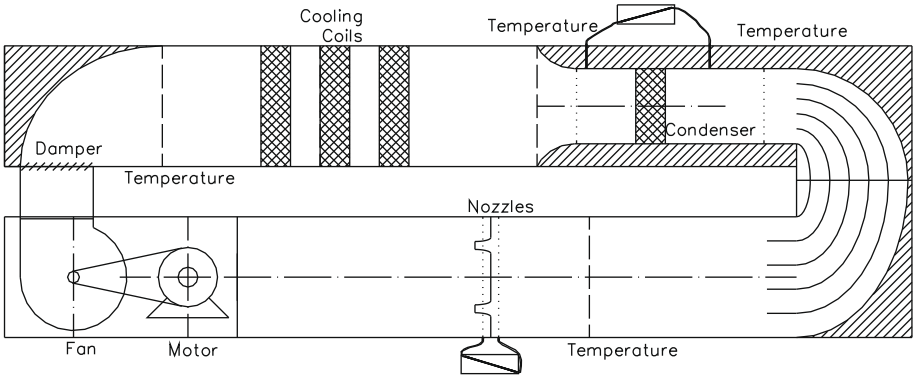

Fig. 9. Test bench.

Table 3
Test conditions.

Variable	Series 1	Series 2	Series 3
Number of tests	76	60	47
Condenser supply pressure	8.5–39.7 bar	10.0–40.4 bar	7.7–38.7 bar
Refrigerant supply temperature	61.9–122.7 °C	55.4–120.3 °C	53.8–107.3 °C
Exhaust temperature (sub-cooling)	20.2–81.8 °C (0.2–33.8 K)	20.7–83.2 °C (5.3–27.4 K)	21.2–87.8 °C (3.0–15.1 K)
Refrigerant mass flow rate	0.055–0.637 kg/s	0.039–0.267 kg/s	0.049–0.223 kg/s
Lubricant flow rate			0.001–0.061 kg/s
Air supply temperature	19–47.3 °C	20–80 °C	15.6–79.1 °C
Air mass flow rate	0.29–2.15 kg/s	0.30–1.84 kg/s	0.51–1. 81 kg/s

by comparison with a Coriolis flow meter, to ±5%. The Coriolis flow rate is not used as reference because it was carried out for a limited number of tests only. In the case where the lubricant flow rate is important, this is calculated as explained in Cuevas et al. [9].

The air-side temperatures are measured according to the ASHRAE Standard 41.1 [1]: the duct cross-sectional area is divided into three horizontal and three verticals parts, which gives nine sections of equal areas. The temperatures are measured in the centre of each section.

The condenser is characterized on the basis of three series of tests, all performed with refrigerant R134a, at the conditions given in Table 3. POE and PAG oils are used in series 1, 2 and 3, respectively. Oil circulation is negligible for the series 1 and 2, but not for the series 3. Figs. 10 and 11 give complementary information about the testing conditions.

The most important test condition is here the condensing pressure: it has been varied in a very large range, up to 40.4 bar at condenser supply, i.e. very near to the critical pressure for this refrigerant (40.6 bar).

4. Validation of the condenser model

4.1. Refrigerant side

4.1.1. Heat transfer

In single phase, heat transfer coefficients are determined with the Shah and London [20] correlation for laminar regime and with the Gnielinski [13] correlation for turbulent regime:

$$Nu_H = 0.488 \cdot (f \cdot Re)^{1/3} \left(\frac{L}{D \cdot Re \cdot Pr} \right)^{-1/3} \tag{19}$$

$$Nu = \frac{(f/8) \cdot (Re - 1000) \cdot Pr}{1 + 12.7 \cdot (f/8)^{1/2} (Pr^{2/3} - 1)} \quad \begin{bmatrix} 0.5 < Pr < 2000 \\ 2300 < Re < 5 \times 10^6 \end{bmatrix} \tag{20}$$

Friction factors are determined with the correlations presented hereafter in Section 4.1.2.

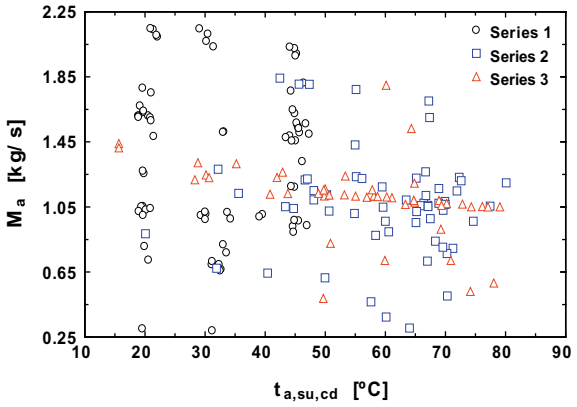

Fig. 10. Domain covered by the testing campaign.

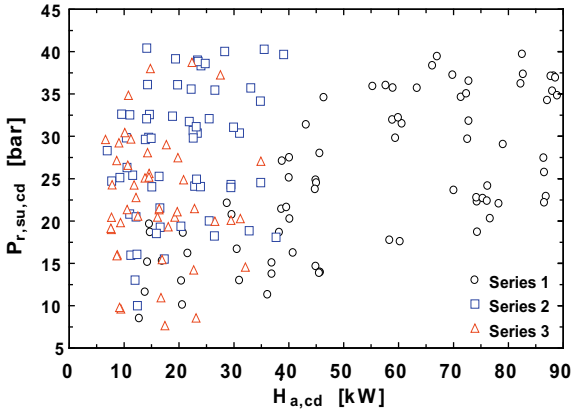

Fig. 11. Domain covered by the testing campaign.

For the two-phase heat transfer coefficient, a correlation for an annular flow is used since, according to the flow pattern maps of Taitel and Dukler [21], Breber et al. [3], Tandom et al. [22] and El Hajal et al. [10], it is the predominant flow pattern at the test conditions achieved in this study.

On the refrigerant side, three correlations proposed, respectively, by Shah [19], Moser et al. [17] and Thome et al. [23] are tried. According to the results, the Thome et al. correlation gives the best agreement between the simulated and our measured values. This is the reason why it is retained, to be compared with our measurements. It is given by the following equations:

$$Nu_{l,\delta} = \frac{h_{tp}\cdot\delta}{k_l} = 0.003\cdot \mathrm{Re}_{l,\delta}^{0.74}\cdot \mathrm{Pr}_l^{0.5}\cdot f_i \tag{21}$$

where δ is the liquid film thickness and $\mathrm{Re}_{l,\delta}$ is the liquid film Reynolds number based on the mean liquid velocity defined by:

$$\mathrm{Re}_{l,\delta} = \frac{4\cdot G\cdot(1-x)\cdot\delta}{(1-\alpha)\cdot\mu_l} \tag{22}$$

δ and f_i, the interfacial roughness factor, are given, respectively, by the following equations:

$$(1-\alpha)\cdot d^2 = (d^2 - (d-2\cdot\delta)^2) \tag{23}$$

$$f_i = 1 + \left(\frac{C_g}{C_l}\right)^{1/2}\cdot\left[\frac{(\rho_l-\rho_g)\cdot g\cdot\delta^2}{\sigma}\right]^{1/4} \tag{24}$$

C_g and C_l are, respectively, the mean vapour velocity and mean liquid velocity in film given by:

$$C_g = \frac{G\cdot x}{\rho_g\cdot\alpha} \quad C_l = \frac{G\cdot(1-x)}{\rho_l\cdot(1-\alpha)} \tag{25}$$

α is the mean void fraction calculated with the following equations:

$$\alpha = \frac{\alpha_h - \alpha_{ra}}{\ln\left(\frac{\alpha_h}{\alpha_{ra}}\right)} \tag{26}$$

$$\alpha_h = \left[1 + \left(\frac{1-x}{x}\right)\cdot\left(\frac{\rho_g}{\rho_l}\right)\right]^{-1} \tag{27}$$

$$\alpha_{ra} = \frac{x}{\rho_g}\cdot\left\{[1+0.12\cdot(1-x)]\cdot\left[\frac{x}{\rho_g}+\frac{1-x}{\rho_l}\right] + \frac{1.18\cdot(1-x)\cdot\left[g\cdot\sigma\cdot(\rho_l-\rho_g)\right]^{0.25}}{G\cdot\rho_l^{0.5}}\right\}^{-1} \tag{28}$$

4.1.2. Pressure drop

Fig. 12 shows the different pressure drops considered in the modelling.

Table 4
Supply and exhaust dimensions.

	Supply	Exhaust
Length (m)	0.56	1.32
Tube diameter (mm)	16	14
Collector diameter (mm)	17.4	17.4
Number of elbows	4	2

$\Delta P_{r,su,cd}$: total (singular and friction) pressure drop at the condenser supply, $\Delta P_{r,cd,i}$: total (singular and friction) pressure drop in the zone i (i = de-superheating, two-phase and subcooled zones), $\Delta P_{r,ex,cd}$: total (singular and friction) pressure drop at the condenser exhaust.

4.1.2.1. Supply pressure drop. Supply pressure drop is decomposed into friction and singular pressure drops mainly located at the elbows and at the collector. The information used to estimate these pressure drops are given in Table 4.

The pressure drop factor for the elbows is 0.84, for the supply collector is 3.4 and for the exhaust collector is 3.76.

In the laminar regime, the friction factor is calculated using the following correlation:

$$f = 64/Re \tag{29}$$

For the turbulent regime, it is calculated with the Colebrook correlation for a tube roughness of 6 μm.

$$\frac{1}{\sqrt{f}} = 1.74 - 0.8686\ln\left(\frac{2\varepsilon}{D_h} + \frac{18.7}{Re\sqrt{f}}\right) \tag{30}$$

Exhaust pressure drop is calculated by using the same procedure.

4.1.2.2. Pressure drop in the de-superheating and sub-cooled zones. Pressure drop in the de-superheating and sub-cooled zones are decomposed in entrance effect, flow acceleration, core friction and exit effect, which are calculated as proposed by Kays and London [15].

The contraction and expansion factors were estimated from Kays and London [15] to 0.4 and 1, respectively, for a ratio of free-flow area to frontal area $\sigma = 0$ and a Reynolds number $Re = \infty$. The number of contractions and expansions are determined from the heat transfer model, which gives the lengths covered for each zone that are afterwards compared to the heat exchanger length.

For the laminar regime, friction factors are calculated using the following correlation:

$$f = 60.3/Re \tag{31}$$

And for the turbulent regime, the Colebrook correlation is used. The heat exchanger wall roughness is estimated to 6 μm. According to the values given by the heat exchanger manufacturer and

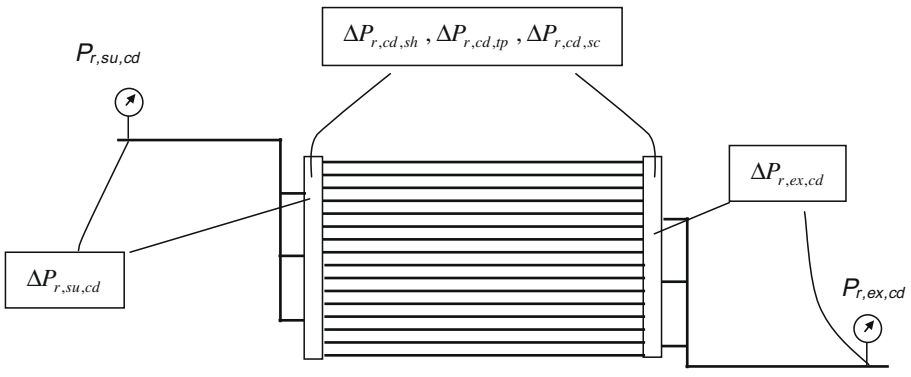

Fig. 12. Refrigerant side pressure drops.

to a parametric study carried out during the simulation, it is the value that gives a better agreement with the measurements. It could be considered as a parameter of the model.

4.1.2.3. Pressure drop in the two-phase zone. Pressure drop in the two-phase zone are also decomposed as explained previously in Section 4.1.2.2. The last three contributions are calculated as proposed by Collier and Thome [6].

The friction pressure drop is calculated using the Friedel correlation [12], which uses a two-phase multiplier given by:

$$\phi_{lo}^2 = A_1 + \frac{3.24 \cdot A_2}{Fr_{tp}^{0.045} \cdot We_{tp}^{0.035}} \tag{32}$$

where the factors A_1 and A_2 are calculated as follows:

$$A_1 = (1-x)^2 + x^2 \cdot \left(\frac{\rho_l}{\rho_g}\right) \cdot \left(\frac{f_{go}}{f_{lo}}\right) \tag{33}$$

$$A_2 = x^{0.78} \cdot (1-x)^{0.24} \cdot \left(\frac{\rho_l}{\rho_g}\right)^{0.91} \cdot \left(\frac{\mu_g}{\mu_l}\right)^{0.19} \cdot \left(1 - \frac{\mu_g}{\mu_l}\right)^{0.7} \tag{34}$$

We_{tp} and Fr_{tp} are the two-phase Weber and Froude numbers:

$$We_{tp} = \frac{G^2 \cdot D}{\rho_h \cdot \sigma} \quad \text{and} \quad Fr_{tp} = \frac{G^2}{g \cdot D \cdot \rho_h^2} \tag{35}$$

This correlation is found to yield the best agreement between the measured and simulated values.

4.1.2.4. Pressure drop in the connections between the heat exchangers. Here, only the friction contribution is considered, because the curvature of the elbows is quite smooth. Fig. 6 shows these connections. The internal diameter of these connections is 10 mm, with a tube length of 0.28 m.

For single phase and in the laminar regime, the friction pressure drops are calculated using the Eq. (29) and for the turbulent regime the friction factor is calculated with Eq. (30) for a tube roughness of 6 μm.

For two-phase flow, pressure drops are calculated using the Friedel correlation given by Eq. (32).

4.2. Air-side

4.2.1. Heat transfer

The air-side heat transfer coefficient is determined with the correlation of Chang and Wang [5] given by the following equation:

$$Nu_{Lp} = Re_{Lp}^{0.51} \Pr^{1/3} \left(\frac{\theta}{90}\right)^{0.27} \left(\frac{F_p}{L_p}\right)^{-0.14} \left(\frac{F_h}{L_p}\right)^{-0.29} \left(\frac{T_d}{L_p}\right)^{-0.23} \left(\frac{L_l}{L_p}\right)^{0.68} \left(\frac{T_p}{L_p}\right)^{-0.28} \left(\frac{F_t}{L_p}\right)^{-0.05} \tag{36}$$

which is valid for a range of Reynolds of $100 < Re_{Lp} < 4000$.

4.2.2. Pressure drop

The air-side pressure drop is determined by using the following equation:

$$\Delta P = \Delta P_{in,core} + \Delta P_{m,core} + \Delta P_{f,core} + \Delta P_{out,core} \tag{37}$$

The core friction factor is calculated using the Chang et al. correlation [4] to be compared with our experimental results. By trial and error, they develop the following equation:

$$f = f_1 \cdot f_2 \cdot f_3 \tag{38}$$

where

$$f_1 = \begin{cases} 14.39 Re_{L_p}^{(-0.805 F_p/F_h)} (ln(1 + (F_p/L_p)))^{3.04} \\ \quad Re_{L_p} \le 150 \\ 4.97 Re_{L_p}^{0.6049 - 1.064/\theta^{0.2}} (ln((F_t/F_p)^{0.5} + 0.9))^{-0.527} \\ \quad 150 < Re_{L_p} < 5000 \end{cases} \tag{39}$$

$$f_2 = \begin{cases} (ln((F_t/F_p)^{0.48} + 0,9))^{-1.435} (D_h/L_P)^{-3.01} (ln(0.5 Re_{L_p}))^{-3.01} \\ \quad Re_{L_p} \le 150 \\ ((D_h/L_P) ln(0.3 Re_{L_p}))^{-2.966} (F_p/L_l)^{-0.7931 (T_p/(T_p - T_h))} \\ \quad 150 < Re_{L_p} < 5000 \end{cases} \tag{40}$$

$$f_3 = \begin{cases} (F_p/L_l)^{-0.308} (F_d/L_l)^{-0.308} (e^{-0.1167 T_p/T_h}) \theta^{0.35} \\ \quad R_{L_p} \le 150 \\ (T_p/T_h)^{-0.0446} ln(1.2 + (L_p/F_p)^{1.4})^{-3.553} \theta^{-0.477} \\ \quad 150 < Re_{L_p} < 5000 \end{cases} \tag{41}$$

Unfortunately, this correlation presents a discontinuity at $Re_{Lp} = 150$. To eliminate this discontinuity, the expression used to calculate f_1 (for $Re_{Lp} < 150$) must be multiplied by a factor of 2.349.

The entrance K_c and exit K_e factors are estimated (from [15] to 0.95 and −0.53 for a $\sigma = 0.76$ and for a laminar regime.

4.3. Modelling results

As explained previously, the modelling is developed by using a "deterministic" approach, i.e. there is no tuning of any parameter to carry out the simulation and the available information of the heat exchanger geometry and correlations from the literature are used to simulate it.

The first result corresponds to the domain covered for the Nusselt and Reynolds numbers and the corresponding heat transfer coefficients on the refrigerant- and on the air-side, presented in Figs. 13–15, and obtained with the correlations given in the previous paragraphs. De-superheating zone works in all tests in turbulent regime and subcooled liquid zone in laminar, transition and turbulent regimes.

Comparisons between modelling and experimental results are presented for the condenser supply pressure in Fig. 16, refrigerant pressure drop in Fig. 17, air-side pressure drop in Fig. 18 and Table 5 presents the average errors, the standard deviations, the minimum and maximum deviations and the confidence limits for the different outputs of the model (which are calculated as

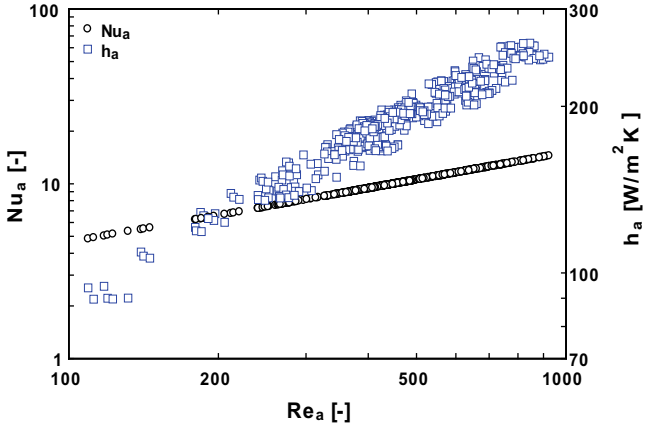

Fig. 13. Domain covered by the actual modelling for the Nusselt, Reynolds and heat transfer coefficients on air-side.

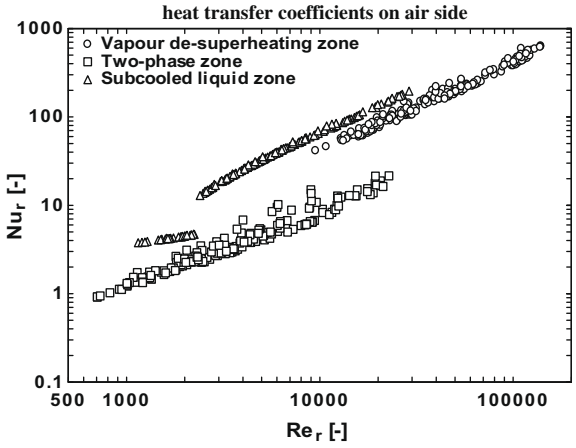

Fig. 14. Domain covered by the actual modelling for the Nusselt and Reynolds number on refrigerant side.

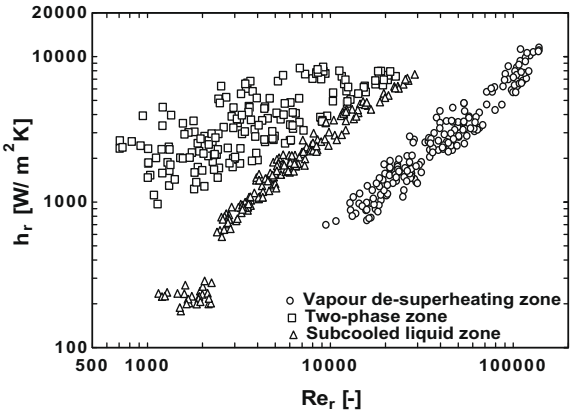

Fig. 15. Domain covered by the actual modelling for the heat transfer coefficients number on refrigerant side.

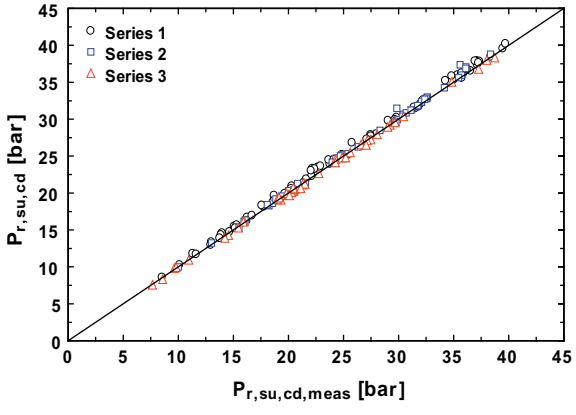

Fig. 16. Simulated versus measured condenser supply pressure.

explained in [9]. As shown in Table 5, the condenser supply pressure is predicted, with a probability of 95%, with a confidence interval of +0.5 and −0.1 bar (that means a condenser power confidence interval of −200 and +100 W); which is here considered as a very good agreement.

Another remark concerns the lubricant circulation: only the results of the series 3 consider the effect of the oil circulation,

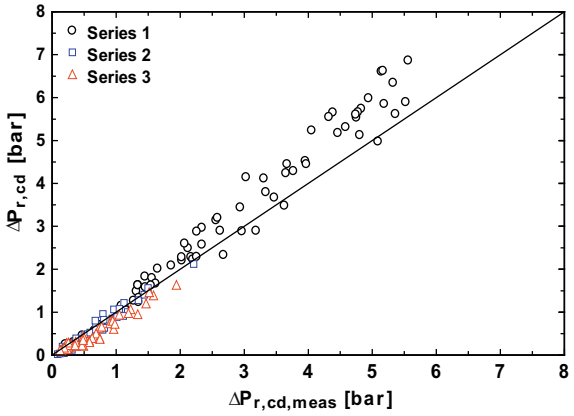

Fig. 17. Simulated versus measured condenser pressure drop.

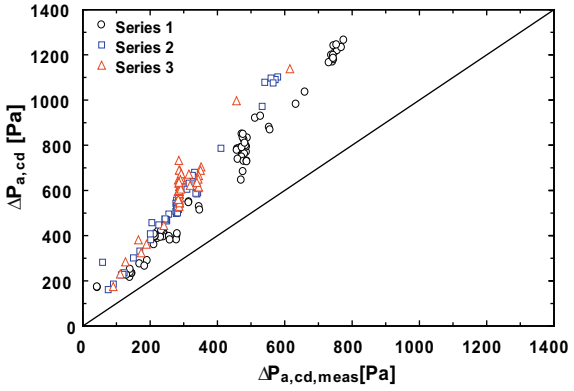

Fig. 18. Simulated versus measured air-side pressure drop.

which is here taken into account in the modelling. According to Fig. 16, no significant effect of the oil circulation is observed on the model results.

Concerning the refrigerant pressure drop, a higher scattering is observed. At low refrigerant pressure drops the model underpredicts the refrigerant pressure drop. It suggests, eventually, an improvement of the model to reduce these errors, but the pressure drop measurement is not very accurate. It is calculated by a difference between two pressures, both of them measured with an accuracy of ±0.2 bar.

The air-side pressure drop is here poorly predicted, it can be attributed to the friction factor correlation used in this study. To fit the experimental with the model results it must be multiplied by a factor of 0.606. That means that the actual pressure losses are 0.606 times lower than the predicted ones. By introducing this correction one could propose a new correlation, based on the Chang et al. [4] model, to determinate the air-side friction factor.

The model principle has been validated in the special case of a louvered fin-and-tube condenser, but this is appropriate to describe other condenser technologies, like plate heat exchanger, tube and fin heat exchanger, etc., and other processes that involve phase change, like evaporators.

5. Conclusions

A condenser "deterministic" model has been presented and validated using experimental data collected on an instrumented condenser made up of five heat exchangers in series on the refrigerant side. The model assumes the condenser is divided into three distinct

Table 5
Error analysis.

Test series	Variable	Average error	Standard deviation	Minimal deviation	Maximal deviation	Confidence interval
1	*Pr,su,cd*	0.4 bar	0.3 bar	−0.1 bar	+1.2 bar	+0.3 bar +0.5 bar
	Ha,cd	−0.039 kW	0.274 kW	−1.258 kW	+0.552 kW	−0.101 kW +0.023 kW
	$\Delta P_{r,cd}$	−0.4 bar	0.5 bar	−0.3 bar	+1.5 bar	+0.3 bar +0.5 bar
	$\Delta P_{a,cd}$	262 Pa	123 Pa	77 Pa	+496 Pa	+234 Pa +289 Pa
2	*Pr,su,cd*	0.2 bar	0.4 bar	−0.2 bar	+1.8 bar	+0.1 bar +0.3 bar
	Ha,cd	−0.143 kW	0.199 kW	−1.155 kW	+0.062 kW	−0.187 kW −0.098 kW
	$\Delta P_{r,cd}$	−0.1 bar	0.1 bar	−0.3 bar	0.2 bar	−0.1 bar −0.1 bar
	$\Delta P_{a,cd}$	268 Pa	107 Pa	+86 Pa	+538 Pa	+244 Pa +292 Pa
3	*Pr,su,cd*	−0.1 bar	0.2 bar	−0.5 bar	+0.3 bar	−0.1 bar −0.1 bar
	Ha,cd	0.053 kW	0.148 kW	−0.104 kW	+0.676 kW	+0.020 kW +0.087 kW
	ΔP_{rcd}	−0.1 bar	0.1 bar	−0.4 bar	0.1 bar	−0.2 bar −0.1 bar
	ΔP_{acd}	308 Pa	87 Pa	+84 Pa	+541 Pa	+289 Pa +328 Pa

zones on the refrigerant side: vapour de-superheating, two-phase and sub-cooled liquid zones. The model is able to determinate the heat transfer power and the pressure drop through each zone.

A very good agreement was observed between the simulated and measured values for the pressures. But, the pressure drops were not very well predicted. Fortunately, the error on the refrigerant pressure drop modelling does not considerably disturb the main outputs of the models that are the condenser supply pressure and power. On the other hand, air-side pressure drop presents a more important difference. However, the latter can be corrected by introducing a multiplication factor of 0.606 in the correlation used for the friction factor. This new correlation can be used to better simulate the results.

The model takes into account the effect of the lubricant circulation. The latter is considered only on the thermal balance, because one assumes that it does not disturb the refrigerant properties and the refrigerant heat transfer coefficient. Here the heat exchanger was tested with a very low, and with an important lubricant circulation. According to the results, no significant variation was observed on the model outputs.

References

[1] ASHRAE Standard 41.1-1986, Standard Method for Temperature Measurement. American Society of Heating, Refrigerating, and Air-Conditioning Engineers, Inc., Atlanta, USA, 1986.

[2] J. Bourdouxhe, M. Grodent, J. Lebrun, A Toolkit for Primary HVAC System Energy Calculations [Computer Program], American Society of Heating, Refrigerating and Air-Conditioning Engineers, Inc., USA, 1995.

[3] G. Breber, J. Palen, J. Taborek, Prediction of horizontal tube side condensation of pure components using flow regime criteria, ASME Journal of Heat Transfer 102 (1980) 471–476.

[4] Y. Chang, K. Hsu, Y. Lin, C. Wang, A generalized friction correlation for louver fin geometry, International Journal of Heat and Mass Transfer 43 (2000) 2237–2243.

[5] Y. Chang, C. Wang, A generalized heat transfer correlation for louver fin geometry, International Journal of Heat and Mass Transfer 40 (3) (1997) 533–544.

[6] J. Collier, J. Thome, Convective Boiling and Condensation, Oxford Science Publications, Oxford, 1996.

[7] C. Cuevas, E. Winandy, Simplified 3 zones modelling of a car air-conditioning condenser, IIR Zero Leakage – Minimum Charge Conference, Stockholm (Sweden), 2002.

[8] C. Cuevas, E. Winandy, J. Lebrun, Modelling of an air condenser working in critical zone for engine cooling by refrigeration loop, In: Vehicle Thermal Management Systems Brighton (UK), May 2003.

[9] C. Cuevas, E. Winandy, J. Lebrun, Testing and modelling of an automotive wobble plate compressor, International Journal of Refrigeration 31 (3) (2008) 423–431.

[10] J. El Hajal, J. Thome, A. Cavallini, Condensation in horizontal tubes, part 1: two-phase flow pattern map, International Journal of Heat and Mass Transfer 46 (2003) 3349–3363.

[11] S. Fischer, C. Rice, The Oak Ridge Heat Pump Models: I. A Steady-State Computer Design Model for Air-to-Air Heat Pumps. Oak Ridge National Laboratory, 1983.

[12] L. Friedel, Improved friction pressure drop correlations for horizontal and vertical two-phase pipe flow. European Two-Phase Flow Group Meeting, Paper E2, Ispra, Italy, 1979.

[13] V. Gnielinski, New equations for heat and mass transfer in turbulent pipe and channel flow, International Chemical Engineering 16 (2) (1976) 359–368.

[14] F. Incropera, D. DeWitt, Fundamentals of Heat and Mass Transfer, third ed., John Wiley & Sons Inc., New Jersey, USA, 1990.

[15] W. Kays, A. London, Compact Heat Exchangers, third ed., McGraw-Hill, New York, USA, 1984.

[16] M. Kempiak, R. Crawford, Three-zone, steady-state modeling of a mobile air-conditioning condenser, ASHRAE Transactions 98 (Part-1) (1992) 475–488.

[17] K. Moser, R. Webb, B. Na, A new equivalent Reynolds number model for condensation in smooth tubes, ASME Journal of Heat Transfer 120 (1998) 410–417.

[18] M. Reichler, Modeling of rooftop packaged air conditioning equipment. M.Sc. Thesis, University of Wisconsin-Madison, 1999.

[19] M. Shah, A general correlation for heat transfer during film condensation inside pipes, International Journal of Heat and Mass Transfer 22 (1979) 547–556.

[20] R. Shah, A. London, Laminar Flow Forced Convection in Ducts. Supplement 1 to Advances in Heat Transfer, Academic Press, New York, USA, 1978.

[21] Y. Taitel, A. Dukler, A model for predicting flow regime transitions in horizontal and near horizontal gas–liquid flow, AIChE Journal 22 (1) (1976) 47–55.

[22] T. Tandom, H. Varma, C. Gupta, A new flow regimes map for condensation inside horizontal tubes, ASME Journal of Heat Transfer 104 (1982) 763–768.

[23] J. Thome, J. El Hajal, A. Cavallini, Condensation in horizontal tubes, part 2: new heat transfer model based on flow regimes, International Journal of Heat and Mass Transfer 46 (2003) 3365–3387.